THE JOURNAL OF PHYSICAL CHEMISTRY A

Article

pubs.acs.org/JPCA

Coupled States in Dinitrofluorene: Relationships between Ground State and Excited State Mixed Valence

Matthew D. Kiesz,[†] Ryan M. Hoekstra,[†] Yen-Ting Chen,[†] João P. Telo,[‡] Stephen F. Nelsen,[§] and Jeffrey I. Zink*,[†]

[†]Department of Chemistry and Biochemistry, University of California, Los Angeles, Los Angeles, California 90095, United States

[‡]Centro de Química Estrutural, Instituto Superior Técnico, Av. Rovisco Pais, 1049-001 Lisboa, Portugal

[§]Department of Chemistry, University of Wisconsin, 1101 University Avenue, Madison, Wisconsin 53706-1396, United States

ABSTRACT: The electronic absorption spectrum of 9,9-dimethyl-2,7-dinitrofluorene radical anion in HMPA displays both a NIR intervalence charge transfer and a visible excited state mixed valence transition. These transitions contain a similar vibronic progression resulting from molecular orbitals that are common to both transitions. Vibrational frequency and intensity data are acquired from the resonance Raman spectrum and used to calculate a best fit for the absorption spectrum. The normal coordinate distortions are analyzed in terms of the electronic changes for both transitions to explain their similarity. The Raman scattering intensity decreases at lower excitation wavelength as a result of Raman de-enhancement caused by interference between neighboring excited states.

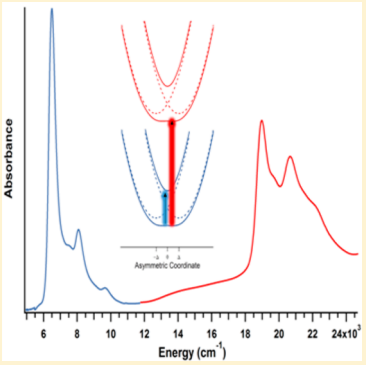

INTRODUCTION

Mixed valence occurs when a radical electron is shared between two equivalent charge bearing units and can occur in both ground and excited states. The theory of electron transfer in mixed valence systems was first developed in the 1960s and applied to transition metal complexes.[1,2] Typical examples of ground state mixed valence contain two charge bearing units, M, and a bridge, B, that covalently links them leading to two unique configurations [M•−B−M] and [M−B−M•] where the radical charge is located on one charge bearing unit or the other.[3−5] Alternatively, a symmetric distribution of the radical charge in the ground state can result in a pair of degenerate yet displaced excited states that couple to produce mixed valence excited states. The time-dependent theory of absorption,[6] resonance Raman,[7,8] and emission spectra have been established and used to interpret and calculate both types of mixed valence and to characterize the coupled states in terms of the distortions along normal coordinates.[9−15] The relative magnitude of the distortions can be measured via a Raman spectrum in resonance with the mixed valence transition. However, in many cases ground state mixed valence absorption bands are low energy (<10 000 cm^{-1}) and difficult to probe directly by resonance Raman spectroscopy.[16−18]

In this paper we examine both ground and excited state mixed valence transitions of 9,9-dimethyl-2,7-dinitrofluorene radical anion, $\mathbf{1}^{\bullet-}$ (Scheme 1), and examine their spectroscopic and theoretical relationship. This compound exhibits a NIR ground state mixed valence band and an excited state mixed valence band in the visible region of the absorption spectrum.[19] The excited state mixed valence transition is probed directly with resonance Raman spectroscopy in order to characterize the excited state in terms of the distortions along multiple normal coordinates. However, the ground state mixed valence is too low in energy to conveniently examine by resonance Raman spectroscopy, but because these bands involve molecular orbitals that are common to both transitions, the ground state mixed valence can be indirectly probed and compared to the excited state.

Scheme 1

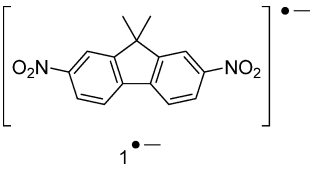

1

THEORETICAL METHODS

The theoretical framework for interpreting the vibrational spectrum and calculating the electronic absorption spectrum is provided by the time-dependent theory of molecular spectroscopy[6] and is briefly presented here. This technique allows for a combination of multiple symmetric and asymmetric normal modes in calculating spectra along with an exact treatment of coupled electronic states.[20,21]

Received: May 29, 2014
Revised: November 11, 2014
Published: November 17, 2014

Absorption Spectra. The primary equation for calculating absorption spectra within time-dependent theory is

$$I(\omega) = C\omega \int_{-\infty}^{\infty} \exp(i\omega t) \times \left\{ \langle \Phi | \Phi(t) \rangle \exp\left(-\Gamma^2 t^2 + \frac{iE_{00}}{h} t \right) \right\} \mathrm{d}t \quad (1)$$

where $I(\omega)$ is the absorption intensity for a given frequency of light, E_{00} is the transition energy at the electronic origin, and Γ is a phenomenological damping factor. The damping accounts for the loss of the wave packet, Φ, to various modes and the bath, and it causes broadening of the absorption spectrum.

The most important component of eq 1 is the autocorrelation function, $\langle \Phi | \Phi(t) \rangle$, which determines the overlap of an initial wave packet with the time evolving wave packet as a function of time. Neglecting mixing of normal coordinates, the total autocorrelation function in a system with k normal coordinates is

$$\langle \Phi | \Phi(t) \rangle = \prod_k \langle \phi^k | \phi^k(t) \rangle \quad (2)$$

where ϕ^k is the wave packet propagating along the kth normal coordinate. In the case of two coupled excited electronic states, ϕ^k bifurcates into two components associated with either state.

The initial wave packet, the eigenfunction of the ground state multiplied by the transition dipole, evolves on the excited surface. In the calculation of excited state mixed valence spectra, where the transition is from $[M-B-M]^-$ to $[M-B-M]^{-}*$, the transition dipole is

$$\mu_d = \begin{pmatrix} 0 & \pm\mu_1 & \mu_2 \\ \pm\mu_1 & 0 & 0 \\ \mu_2 & 0 & 0 \end{pmatrix} \quad (3)$$

where μ_i is the transition to either diabatic surface. The molecular structure dictates the relative sign of the transition dipole such that a positive sign implies parallel units whereas a negative sign implies antiparallel units that are oriented 180° apart from the linking bridge. Appropriate weighting of parallel (I_p) and antiparallel (I_a) spectra allow for calculation of spectra of molecules at intermediate angles:[23]

$$\frac{I_a}{I_p} = \frac{\mu_a^2}{\mu_p^2} = \left(\tan\frac{\beta}{2} \right)^2 \quad (4)$$

where β is the angle between the charge bearing units. Alternatively, in calculating intervalence charge transfer (IVCT) spectra, where the transition is between M^-–B–M and M–B–M^-, the transition dipole has the form

$$\mu_{d,IV} = \begin{pmatrix} 0 & \mu(Q) \\ \mu(Q) & 0 \end{pmatrix} \quad (5)$$

such that the components of the ground state eigenfunction associated with each diabatic surface are evolved on the other surface. The off-diagonal components may be a function of the configurational coordinate, Q, to reflect the selection rules of a given transition (e.g., vibronically allowed).

When a wave packet evolves on coupled excited states, the time evolved components on both surfaces must be determined. The time-dependent wave packet is given by the time-dependent Schrödinger equation:

$$i\frac{\partial}{\partial t}\begin{pmatrix} \phi_1 \\ \phi_2 \end{pmatrix} = \begin{pmatrix} H_1 & V_{12} \\ V_{21} & H_2 \end{pmatrix}\begin{pmatrix} \phi_1 \\ \phi_2 \end{pmatrix} \quad (6)$$

where H_i move the wave packet along the coordinate and the off-diagonal V_{ij} transfer amplitude between the states. The diagonal components of the total Hamiltonian are

$$H_i = -\frac{1}{2M}\nabla^2 + V_i(Q) \quad (7)$$

The potential energy operators, $V_i(Q)$, are most often modeled as harmonic potentials which are displaced an equal amount in opposite directions along an asymmetric normal coordinate.

$$V_i(Q) = \frac{1}{2}k_i(Q \pm \Delta Q)^2 \quad (8)$$

The force constant is $k_i = 4\pi^2 M(\hbar\omega_i)^2$, and ω_i is frequency along the specified coordinate. The overlap is given by

$$\langle \phi | \phi(t) \rangle = \langle \phi_1 | \phi_1(t) \rangle + \langle \phi_2 | \phi_2(t) \rangle \quad (9)$$

Propagating wave packets and calculating spectra according to the equations and procedures outlined here provide a versatile framework that permits various functional forms of the off-diagonal diabatic coupling, V_{12}, the potential energy operator, and the transition dipole operator. Furthermore, the calculations carried out in this paper are carried out exactly according to the time-dependent Schrödinger equation where amplitude is transferred between potential surfaces at every time step, not in an adiabatic basis set where the potential energy Hamiltonian is diagonalized.

EXPERIMENTAL SECTION

The dinitrofluorene compound was synthesized by known procedures.[19,22] To produce the radical anion, the compound was reduced in vacuum-sealed glass cells equipped with a quartz optical cell by contact with 0.2% Na–Hg amalgam in the presence of excess [2,2,2]-cryptand. The absorption spectrum was checked to confirm formation of the radical anion, taken at room temperature with a Cary 5000 UV–vis–nIR spectrophotometer. Raman spectra were collected with a triple monochromator equipped with a Princeton Instruments LN-CCD and excited over multiple visible lines of a Coherent krypton ion laser and argon ion laser at powers less than 50 mW to avoid photodegradation.

RESULTS

Absorption Spectroscopy. The hexamethylphosphoramide (HMPA) solution absorption spectrum of $\mathbf{1}^{\bullet-}$ in the visible and near-IR wavelength region is shown in Figure 1. The low-energy transition has a maximum at 6890 ± 20 cm^{-1} (1450 nm) and shoulders at 7930 ± 100, 8500 ± 100, and 10090 ± 100 cm^{-1}. The visible transition has a peak maximum at 18 980 ± 50 cm^{-1} (527 nm) and shoulders at 19 670 ± 150, 20 660 ± 100, and 22 150 ± 200 cm^{-1}.

Resonance Raman Spectroscopy. Resonance Raman spectra were collected by a triple monochromator and detected with a CCD. Solutions of $\mathbf{1}^{\bullet-}$ in HMPA were excited by argon and krypton ion lasers at wavelengths of 465, 476, 496, 514, and 530 nm. Peak intensities were numerically integrated and normalized to solvent peaks. The data obtained from 530.9 nm excitation are summarized in Table 1, including experimental and calculated frequencies, intensities, and assignments.

dx.doi.org/10.1021/jp505299p | J. Phys. Chem. A 2014, 118, 11490–11498

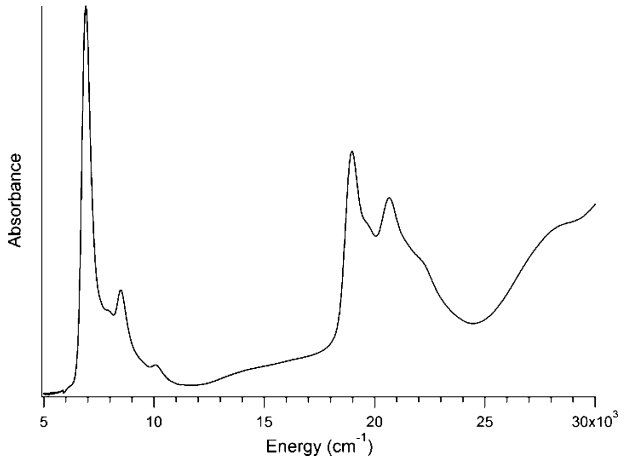

Figure 1. Absorption spectrum of $\mathbf{1}^{\bullet-}$ in HMPA.

Table 1. Raman Frequencies, Intensities, Distortions, and Assignments for Vibrations Observed upon 530 nm Excitation of $\mathbf{1}^{\bullet-}$

calcd ω (cm^{-1})	exptl ω_{530} (cm^{-1})	rel int[a]	Δ_s[b]	Δ_a[c]	assignment
238	229	5.11	1.20	0.99	aryl−aryl stretch
537	537	2.40	0.35	0.30	C−N wag
601	597	2.31	0.30	0.27	aryl−aryl rock
753	724	6.63	0.43	0.34	aryl distortion, ONO bend
875	860	9.38	0.43	0.35	aryl breathing
951	880	1.14	0.12	0.14	aryl distortion
1141	1116	5.28	0.26	0.23	C−H wag, CN stretch
1367	1330	12.49	0.32	0.27	CN stretch
1390	1356	6.99	0.24	0.18	CN, C=C stretch
1485	1452	2.72	0.13	0.11	CN, C=C stretch
1584	1482	4.15	0.17	0.15	CN, C=C stretch
1625	1582	19.10	0.33	0.40	C=C stretch

[a]Intensities were scaled relative to a 630 cm^{-1} vibration of the solvent, HMPA. [b]The relative distortions, Δ_s, were calculated using Savin's formula. [c]The distortions, Δ_a, were used to calculated the best fit absorption spectrum.

DISCUSSION

Neighboring Orbital Model. The sign of the coupling is rarely considered for ground state mixed valence complexes since the adiabatic potential energy surfaces depend on the square of the coupling.[2,23,24] Furthermore, since one of these two states is symmetric and the other is asymmetric, the transition between them is inherently Laporte allowed. However, the spectrum for a transition from a delocalized ground state to a mixed valence excited state has two bands (one to either adiabatic state), and only one will be allowed. The sign of the coupling has been evaluated in terms of how the excited state wave functions interact as interpreted by the neighboring orbital model.[23] The neighboring orbital model (NOM) considers how specific frontier orbitals of the charge bearing units interact.[24] For the majority of examples that have been studied, the sign of the coupling was positive (i.e., the out-of-phase combination of the charge bearing units was more stable).[23,25−29] This previously unexplained phenomenon results from the electronic interactions via the bridging unit—the orbitals on the bridge that are energetically the nearest neighbors to the orbitals on the charge bearing unit combined in such a way to stabilize the out-of-phase combination.[25−29]

In the case of $\mathbf{1}^{\bullet-}$ the coupling is negative. The nitrobenzene π^* orbitals that are the diabatic orbitals that interact to form the frontier molecular orbitals of $\mathbf{1}^{\bullet-}$ are shown in the NOM diagram in Figure 2. The molecular orbitals were calculated in Gaussian 09 using the B3LYP/6-31G* method, and the results were imaged by GaussView 5.[30] The coupling between the nitrobenzene charge bearing units occurs directly via the C−C bridging bond, and the in-phase combination is lower in energy as represented by the singly occupied molecular orbital

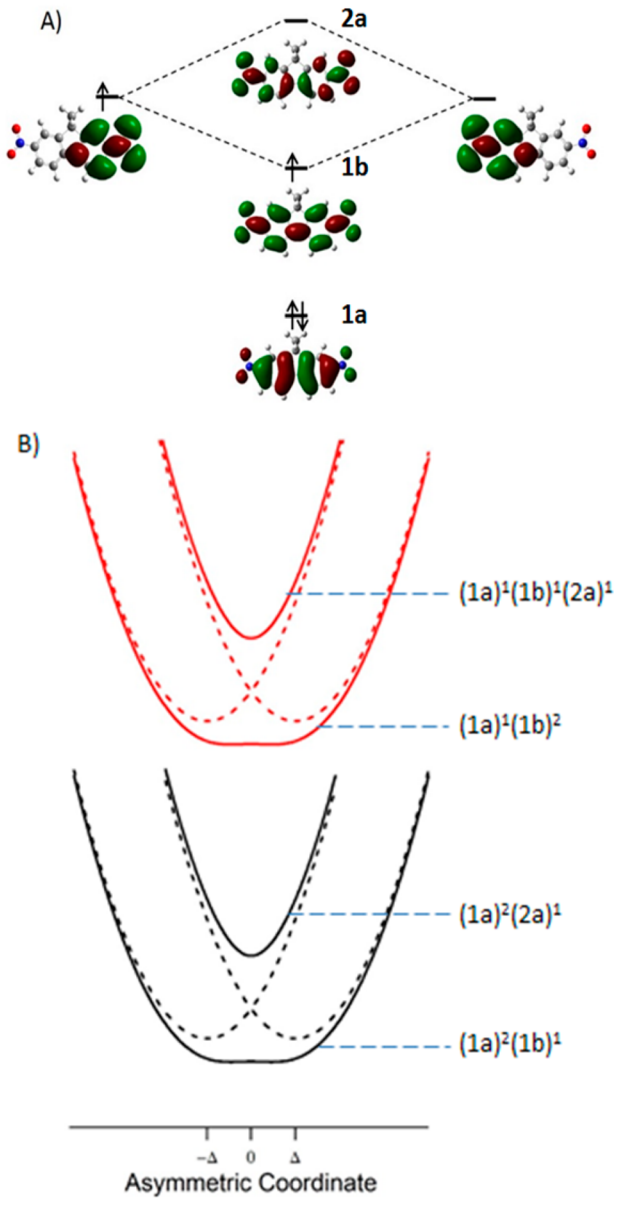

Figure 2. (A) Neighboring orbital model diagram of $\mathbf{1}^{\bullet-}$. Left- and right-hand sides depict diabatic orbitals of the two nitrobenzene charge bearing units. The center column displays the in-phase and out-of-phase combinations of the charge bearing units as well as the HOMO. Orbitals are labeled with their irreducible representations under C_2 symmetry. (B) Potential energy surfaces along an asymmetric coordinate used to model electronic states. Solid lines depict adiabats, and dashed lines depict diabats. Electronic configurations are given beside each adiabat.

dx.doi.org/10.1021/jp505299p | J. Phys. Chem. A 2014, 118, 11490−11498

(SOMO). Similarly, the higher energy out-of-phase combination of the diabatic orbitals forms the LUMO.

In $\mathbf{1}^{\bullet-}$ the nitrobenzene π^* in-phase and out-of-phase combinations correspond to the SOMO and LUMO, respectively, indicating that the coupling is negative. This implies that in a two-state model the lower surface corresponds to an in-phase combination while the upper surface corresponds to an out-of-phase combination. Since the HOMO is asymmetric with respect to the interchange of the two charge bearing units, the transition to the symmetric in-phase combination (the SOMO) is allowed while the transition to the asymmetric higher energy out-of-phase combination is forbidden.

The preponderance of positive coupling in previously analyzed systems has led to confusion with a different type of coupling, through space dipole coupling such as exciton coupling.[25,26,31] In the molecular exciton model, neighboring transition dipoles within dimers couple, forming a new set of electronic states that are similarly in-phase and out-of-phase combinations of the monomer's transitions.[32,33] The resulting states and their corresponding selection rules have been summarized by Kasha for the possible arrangements of dimers. The case of two molecules with collinear dipoles is similar to the arrangement of the nitrobenzenes in $\mathbf{1}^{\bullet-}$ (Figure 3). The

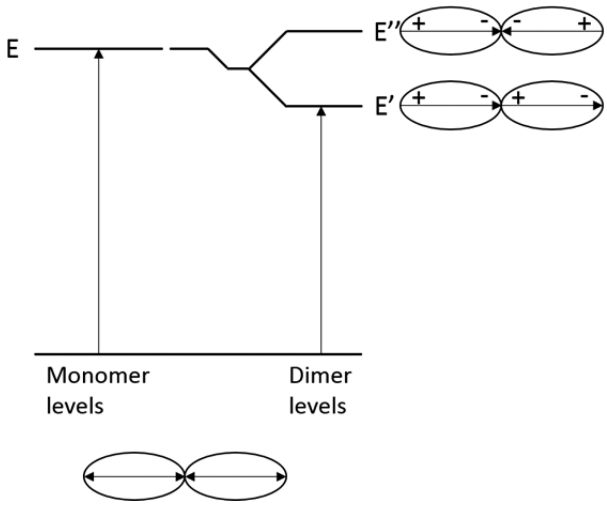

Figure 3. Energy level diagram for coupled excitons in a dimer.

electronic transition of the monomer is shown on the left-hand side of the diagram. In a dimer the transition dipoles couple to form the two states E′ and E″. The identity of these states can be determined by considering the electrostatic interaction of the transition dipoles in this collinear arrangement. The two unique combinations are a head-to-head and a head-to-tail combination. Because the head-to-tail combination has an attractive Coulombic interaction, it is the lowest energy state, E′. The transition dipoles constructively add to produce an allowed transition with approximately double the intensity. In contrast, the head-to-head combination has a repulsive interaction which leads to the higher energy state E″, and this arrangement of the transition dipoles cancels out leading to an electric dipole forbidden transition.[33]

There are two significant differences between the neighboring orbital model and the molecular exciton model. Primarily, the molecular exciton model is through-space coupling between the transition dipoles and requires that the "*electron overlap between the light absorbing units must be small*".[33] In contrast, the NOM specifically couples the electronic wave functions of the light absorbing units since the electron overlap is large. Second, for molecules in a collinear arrangement the molecular exciton model requires that the effective sign of the coupling is positive while the sign of the coupling from the NOM is dictated by the interaction of the individual orbitals of the covalent bridge and the charge bearing units. In the case of $\mathbf{1}^{\bullet-}$, the NOM indicates that the sign of the coupling is negative, demonstrating a difference from the molecular exciton model.

Absorption Spectrum Assignment. The electronic absorption spectrum of $\mathbf{1}^{\bullet-}$ displays two intense transitions at 6894 and 18 975 cm^{-1}. The lowest energy transition is assigned as the ground state mixed valence (GSMV). In the NOM (adiabatic picture) this corresponds to moving the electron from the SOMO to the LUMO. The higher energy transition is assigned as the excited state mixed valence charge transfer where an electron is removed from the HOMO and placed in either the SOMO or the LUMO.

Two aspects of the HOMO to SOMO and SOMO to LUMO absorptions are consistent with these assignments. First, the vibronic spacings of these transitions are similar as both transitions involve populating or depopulating ring orbitals. Because both of these transitions involve similar diabatic orbitals, it is expected that the absorption spectra will show similar progressions. Second, the patterns for the relative intensity of the vibronic peaks are similar and support the hypothesis that the same types of orbitals are involved in both transitions.

Important Symmetric Modes. The presence of highly distorted symmetric modes in electronic transitions adds vibronic structure and overall width to the absorption spectrum.[34] In contrast to a mode with a small distortion that will produce a very sharp spectrum, a highly distorted mode will contribute intensity to vibronic sidebands on the high enegy side of the origin, therefore leading to broader spectrum overall. In the case of small distortion, only the lowest energy vibrational level has any significant overlap, and a sharp absorption is observed; highly distorted modes display much larger overlap for higher vibrational levels, yielding a broadened spectrum. These highly distorted modes can be observed and their relative distortions calculated from the resonance Raman spectrum.

Raman spectra collected in resonance with the excited state mixed valence HOMO to SOMO transition displayed many enhanced vibrational modes. The vibrations that were greater than 5% intensity of the most intense vibration were chosen for further analysis. From the relative intensities, relative dimensionless distortions can be calculated via Savin's formula[35,36] (Table 1). These distortions correspond to the geometrical changes that occur in the molecule when it is excited from the ground to an excited state. The specific coordinates that are most distorted will correspond to regions that have changes in electron density or changes in the bonding/antibonding interactions. These changes in the bonding interactions will cause geometrical distortions such as bond length or angle changes which are distortions along one or more normal coordinates.

How can we interpret from the molecular orbitals specifically which normal modes are enhanced in the resonance Raman spectrum of $\mathbf{1}^{\bullet-}$? In promoting an electron from the HOMO to the SOMO level, an electron is moved from an out-of-phase combination of nitrobenzene orbitals to the in-phase

combination of the diabatic nitrobenzene π^* orbitals (Figure 4). Analyzing the specific changes in nodal structure and electron density will dictate which normal coordinates will be distorted in the excited electronic state.

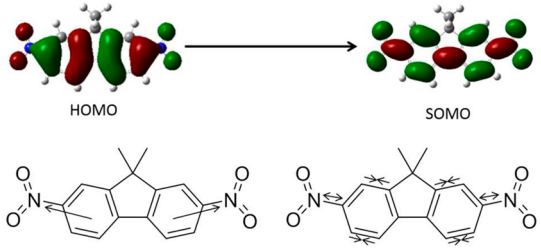

Figure 4. Top: HOMO and SOMO orbitals of $\mathbf{1}^{\bullet-}$. Bottom: representative displacement vectors for a 229 cm^{-1} (left) and 1582 cm^{-1} (right) normal modes of $\mathbf{1}^{\bullet-}$.

The HOMO has significant antibonding character of the π system along three vertical nodes. There is one node within the ring of both nitrobenzene charge bearing units and a third node between the two charge bearing units. While the SOMO is similarly an antibonding orbital of the π system, the specifics of the nodal structure change as individual bonds change from bonding to antibonding, and *vice versa*. Most importantly, the interaction between the two charge bearing units changes from antibonding to bonding and the N−C bond becomes more strongly bonding.

By identifying the changes in electron density, it is expected that the most enhanced modes in the resonance Raman spectrum will have large distortions along the carbon−carbon double bonds in the rings and the C−C bond connecting the nitrobenzene units. The phases of the displacements can also be rationalized from this picture. Since all the carbon−carbon double bonds change strength in the HOMO−SOMO transition, one of the highly distorted modes should display simultaneous in-phase contractions along these bonds. Modes showing large distortions along the nitrogen−carbon bonds should also be distorted and enhanced in the Raman spectrum. DFT calculations of $\mathbf{1}^{\bullet-}$ predict a normal mode at 1624 cm^{-1}, consistent with in-phase contractions along the carbon−carbon double bonds and the carbon−nitrogen bonds as expected. Accordingly, there is an intense vibration in the resonance Raman spectrum at 1582 cm^{-1} that is assigned to this normal mode. The other most enhanced normal mode of $\mathbf{1}^{\bullet-}$ is observed at 229 cm^{-1} and assigned to a normal mode in which the two nitrobenzene units rock toward and away from each other. This motion is driven by the increased bonding interaction between the two phenyl rings but is more difficult to interpret since the distortion is not occurring directly along the bond axes.

Calculating the Absorption Spectrum. The band shape of the absorption spectra for the transitions involving the mixed valence system of $\mathbf{1}^{\bullet-}$ can be calculated using eq 1 and the distortion data derived from the resonance Raman spectra. However, the enhanced vibrations observed in the resonance Raman spectrum are all symmetric. Calculating a spectrum using only these normal coordinates neglects the asymmetric coordinate of a mixed valence system. Since the system is highly delocalized, the vibronic structure is a result of the progression of the symmetric modes, and the asymmetric coordinate does not contribute to the band shape.[28]

The visible region of the absorption spectrum includes at least two prominent transitions. The more dominant transition that peaks near 18 980 cm^{-1} is assigned to the HOMO to SOMO transition. However, the breadth and intensity on the high-energy side of the visible band cannot be accounted for by a single electronic transition. Calculating both the absorption spectrum and the resonance Raman profiles will demonstrate the presence of a second electronic transition near 20 000 cm^{-1}. Since the SOMO → LUMO transition is near 7000 cm^{-1}, the HOMO → LUMO transition should similarly be found approximately 7000 cm^{-1} above the HOMO → SOMO transition. This is far beyond the visible region of the absorption spectrum and indicates that other orbitals must be involved. The second electronic transition therefore most likely originates from an orbital that is more stabilized than the HOMO and places an electron in the SOMO. The HOMO−3 orbital contains significant electron density on the benzene rings and is a likely candidate for the origin of the additional electronic transition.

The distortions for the most intense Raman vibration modes collected in resonance with the visible band were calculated using Savin's formula. Using the relative distortions calculated from Savin's formula, Δ_s, we can calculate an absorption fit for the primary component of the visible band, with the electronic origin at 18 920 cm^{-1}. After optimizing the magnitude of the distortions within experimental error of the Raman intensity (Δ_a), we produced a calculated absorption spectrum that displays some of the vibronic features of the experimental spectrum (Figure 5a). However, the intensity on the higher energy side of the spectrum is not reproduced. Some of the intensity in this region is due to the tail of an intense UV transition not shown in this figure, although this cannot account for all of the excess intensity in this region.

The second discrepancy with this fit is the large vibronic feature that appears near 1685 cm^{-1} from the E_{00}. The presence of this vibronic feature cannot be easily explained since there is no observed Raman vibrational mode at that frequency, and the nearest enhanced mode is at 1582 cm^{-1}. While decreases in frequency between the ground and excited state are common, a 100 cm^{-1} increase in vibrational frequency is unusual. Excited state vibrations are often at lower frequencies than ground state vibrations since ground to excited state transitions normally remove an electron from a bonding orbital and place it in an antibonding orbital. However, the assigned HOMO → SOMO transition significantly changes the π structure from antibonding to bonding along several bonds. Specifically, all of the bonds that change from π^* to π have significant distortion in the 1582 cm^{-1} mode, justifying a large increase in the vibrational frequency of the 1582 cm^{-1} mode. Yet even a large adjustment of this vibrational frequency does not produce a satisfactory fit of the experimental absorption spectrum in this region.

Including a second electronic transition in the calculated absorption spectrum would account for the vibronic feature at 1685 cm^{-1} from E_{00} and also account for the intensity on the high-energy side of the spectrum. As earlier discussed, this higher energy transition likely corresponds to the HOMO−3 to SOMO transition. However, the interference of the Raman scattering in the region where the two visible transitions overlap prevents the calculation of distortions that correspond to the second transition. These effects of a second state on the Raman signal will be explained further in the next section. Therefore, without the distortion values needed, we do not show a total calculated absorption spectrum including the second transition.

dx.doi.org/10.1021/jp505299p | J. Phys. Chem. A 2014, 118, 11490−11498

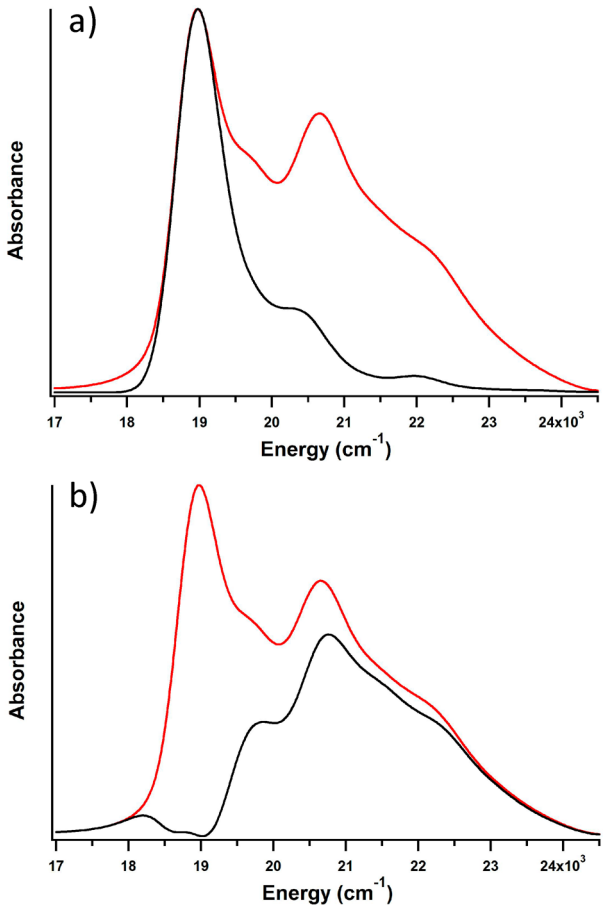

Figure 5. (a) Baseline subtracted experimental (red) and calculated (black) absorption spectra of the visible band of $\mathbf{1}^{\bullet-}$. (b) Difference in intensities between experimental absorption spectrum (red) and the HOMO → SOMO absorption band fit, showing a higher energy second transition (black).

Instead, shown in Figure 5b is the difference in intensities between the experimental absorption spectrum and the calculated absorption spectrum, which provides a clear picture on the presence of a second band at higher energy.

As earlier discussed, both the GSMV and the visible band transitions involve populating or depopulating molecular orbitals with electron density mainly on the ring. This results in similar enhanced vibrations and the observed resemblances in the vibronic spacing and suggests that the two transitions have comparable distortion values. To test our hypothesis that the properties are related, we fit the GSMV experimental absorption using the same set of vibrational mode frequencies acquired from resonance Raman in the visible region, but with freely adjusted distortion values in order to find the optimum set of relative distortions to achieve a good fit (shown in Figure 6).

The optimized values are shown in Table 2, and a comparison of these with the distortion values acquired from experiment and used to fit the visible band reveal their close similarity. A generic mode at frequency 3100 cm^{-1} has been included for both ESMV and GSMV bands to model the multiple CH and NH modes,[37] with a total distortion modeled at 0.2. Overall, the relative values of the distortions are very similar and confirm our hypothesis that due to similar orbitals being involved in the two transitions, the set of distortion values are comparable.

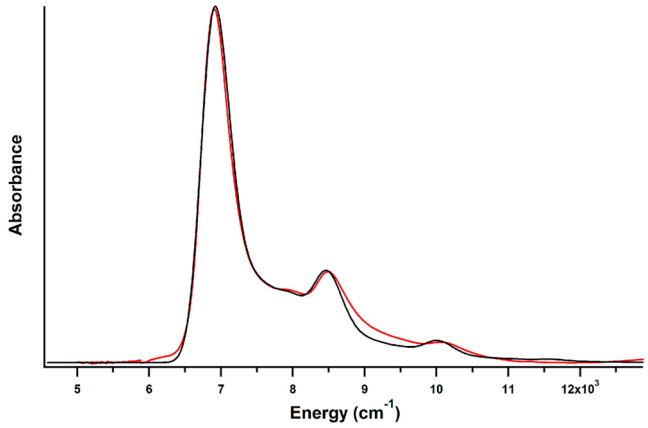

Figure 6. Experimental (red) and calculated (black) absorption spectra of the low-energy band of $\mathbf{1}^{\bullet-}$.

Table 2. Raman Frequencies and Distortions for Calculated Fit of GSMV Absorption Band, in Comparison to Distortions for ESMV Fit

ω (cm^{-1})	Δ (GSMV)	Δ (ESMV)	ω (cm^{-1})	Δ (GSMV)	Δ (ESMV)
229	0.92	0.99	1330	0.19	0.27
537	0.32	0.30	1356	0.05	0.18
597	0.33	0.27	1452	0.05	0.11
724	0.28	0.34	1482	0.05	0.15
860	0.24	0.35	1582	0.55	0.40
880	0.25	0.14	3100	0.2	0.2
1116	0.41	0.23			

Interference Effects in Resonance Raman Profiles. The Raman profiles of $\mathbf{1}^{\bullet-}$ across the visible region provide additional evidence for the presence of a second excited state. Figure 7a shows three Raman spectra of $\mathbf{1}^{\bullet-}$ excited at 530, 496, and 465 nm (normalized to the 630 cm^{-1} HMPA peak), and Figures 7b and 7c show the Raman profiles of the 229 and 1582 cm^{-1} modes, respectively. There is a large decrease in the relative scattering intensity as the excitation wavelength decreases. Raman profiles plot the relative Raman scattering intensities of a mode as a function of excitation wavelength and generally do not deviate from the contour of the absorption spectrum as much as observed here. We will show here that the large deviation is a Raman de-enhancement that is the result of a second state nearby.

In contrast to the absorption spectrum that is the sum of the intensities of multiple overlapping excited states, Raman scattering squares the sum of the polarizabilities of the excited states.[39,40] The effect of this produces an interference between neighboring excited states, and thus the Raman profile may not mimic the shape of the absorption spectrum. Instead, the real and imaginary components of the polarizability from the nearby states can effectively cancel out, causing a Raman de-enhancement.[41] This has previously been demonstrated in organometallic sandwich complexes and in other compounds displaying mixed valence excited states.[39,42−44]

The presence of a second excited state within the visible region can be inferred by the de-enhancement of the intensities in the Raman profiles. The Raman profiles of the 229 and 1582 cm^{-1} modes of $\mathbf{1}^{\bullet-}$ demonstrate the presence of the second excited state. The experimental Raman profile of the 229 cm^{-1} mode has a maximum at 18 868 cm^{-1} excitation and decreases rapidly as the excitation energy is increased but has a slight

dx.doi.org/10.1021/jp505299p | J. Phys. Chem. A 2014, 118, 11490−11498

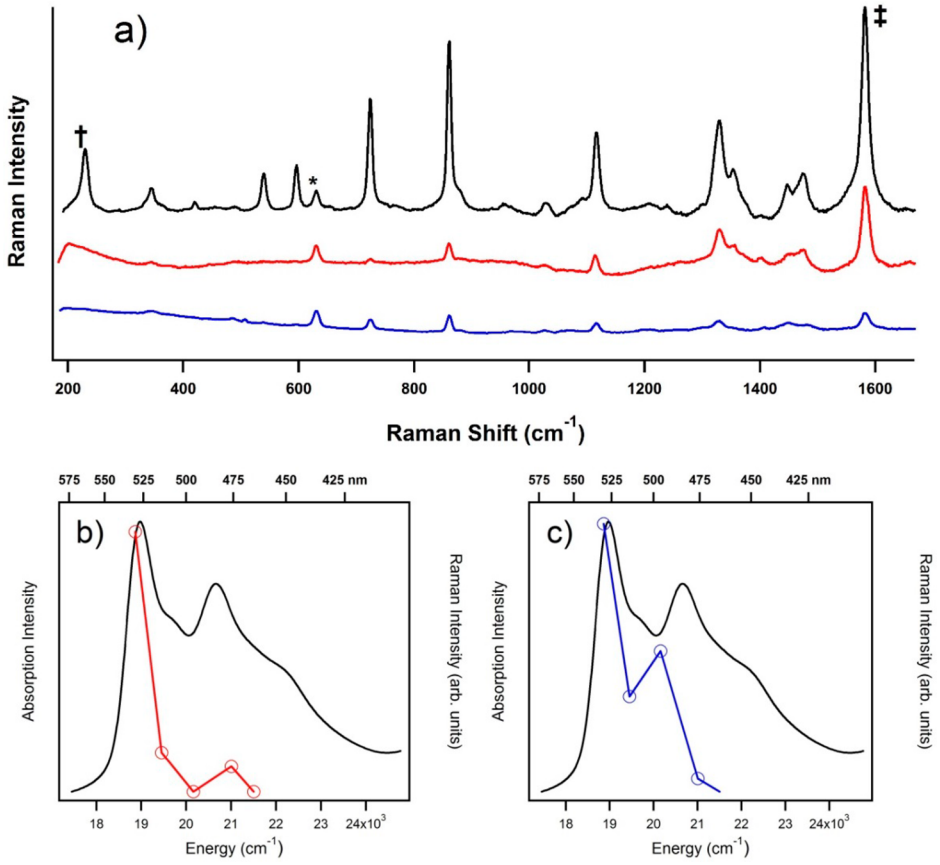

Figure 7. (a) Raman spectra excited at 530 nm (black), 496 nm (red), and 465 nm (blue). All spectra are normalized to the 630 cm^{-1} solvent peak (∗). The 229 cm^{-1} peak (†) and 1582 cm^{-1} peak (‡) are denoted. Bottom: Raman profiles (corrected for self-absorption[38]) of 229 cm^{-1} (b) and 1582 cm^{-1} (c) modes of $\mathbf{1}^{\bullet-}$. The experimental intensities are marked by circles and squares for the 229 and 1582 cm^{-1} modes, respectively.

increase in the scattering intensity near 21 000 cm^{-1}. Similarly, the Raman profile of the 1582 cm^{-1} mode closely follows the absorption spectrum at lower energies with a maximum intensity near 18 868 cm^{-1}. However, the scattering intensity of the 1582 cm^{-1} sharply drops off and has a minimum and does not regain its intensity at higher energy. The loss of Raman intensity, which does not follow the absorption spectrum, is a result of the Raman de-enhancement induced by the presence of a nearby excited state.

The potential of neighboring excited states to cause Raman de-enhancement can be demonstrated via a pedagogical example to demonstrate how the polarizabilities from neighboring states can cancel out. Examining plots of the polarizabilities for the 1582 cm^{-1} mode shown in Figure 8 demonstrates the origin of the Raman de-enhancement. Between 21 000 and 21 500 cm^{-1}, near the electronic origin of the second excited state, both the real components and imaginary components of each state are opposite in sign. Adding them thus diminishes the intensity of either one alone, producing the observed de-enhancement in the Raman profile.

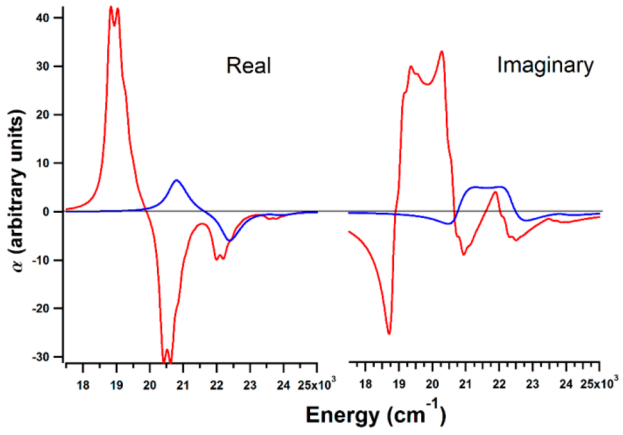

Figure 8. Left: real components of the polarizability for state 1 (red) and state 2 (blue). Right: imaginary components of the polarizability.

CONCLUSION

The electronic absorption spectrum of $\mathbf{1}^{\bullet-}$ contains two bands that are characteristic of ground state and excited state mixed valence. The NIR transition corresponds to the IVCT associated with ground state mixed valence while the energy of the transition to the mixed valence excited state is in the visible region. The similar vibronic progressions in both of these bands is a result of the molecular orbitals that are in common with these transitions.

The neighboring orbital model of $\mathbf{1}^{\bullet-}$ demonstrates that a set of orbitals localized on the nitrobenzene units combine in-phase and out-of-phase to form the SOMO and LUMO molecular orbitals, respectively. Furthermore, the in-phase combination, the SOMO, is lower in energy than the out-of-phase combination, implying that the coupling between the nitrobenzene is negative. The molecular exciton model predicts that chromophores interacting in this geometry will result in positive coupling. This difference in the sign of the coupling for

dx.doi.org/10.1021/jp505299p | J. Phys. Chem. A 2014, 118, 11490−11498

$1^{\bullet-}$ demonstrates how the excited state mixed valence model is distinct from the molecular exciton model.

Raman spectra collected in resonance with the transition to the mixed valence excited state were used to determine the distortions along symmetric normal coordinates of $1^{\bullet-}$. In particular, the 229 and 1582 cm^{-1} vibrations were the most intense in the resonance Raman spectrum and therefore the most distorted coordinates in the excited state. However, as the excitation wavelength was decreased, the Raman intensity of several vibrations decreased significantly due to Raman de-enhancement. The interaction between nearby excited states caused the polarizability terms to cancel and greatly reduced the Raman scattering.

Fitting both of the transitions that correspond to the ground state and excited state mixed valence showed that the 229 and 1582 cm^{-1} vibrations contributed significantly to the overall width and vibronic progression of both bands. This relationship in the normal coordinate distortions and electronic absorption spectra of the two transitions is not coincidental. It is a result of the fact that both transitions change the population of the SOMO, leading to similar geometric distortions as a relationship between ground state mixed valence and excited state mixed valence.

AUTHOR INFORMATION

Corresponding Author

*Tel 1-310-825-1001; e-mail zink@chem.ucla.edu (J.I.Z.).

Notes

The authors declare no competing financial interest.

ACKNOWLEDGMENTS

Funding for M.D.K. and Y.-T.C. by the Research and Student Support Fund is gratefully acknowledged.

REFERENCES

(1) Day, P.; Hush, N. S.; Clark, R. J. H. Mixed Valence: Origins and Developments. *Philos. Trans. R. Soc. A* **2008**, *366*, 5−14.

(2) Brunschwig, B. S.; Creutz, C.; Sutin, N. Optical Transitions of Symmetrical Mixed-Valence Systems in the Class II-III Transition Regime. *Chem. Soc. Rev.* **2002**, *31*, 168−184.

(3) Creutz, C. Mixed Valence Complexes in d^5-d^6 Metal Centers. *Prog. Inorg. Chem.* **1983**, *30*, 1−74.

(4) Crutchley, R. J. Intervalence Charge Transfer and Electron Exchange Studies of Dinuclear Ruthenium Complexes. *Adv. Inorg. Chem.* **1994**, *41*, 273−325.

(5) Bunting, P.; Chisholm, M. H.; Gallucci, J. C.; Lear, B. J. Extent of M_2 δ to Ligand π-Conjugation in Neutral and Mixed Valence States of Bis(4-isonicotinate)-bis(2,4,6-triisopropylbenzoate) Dimetal Complexes (MM), Where M = Mo or W, and Their Adducts with Tris(pentafluorophenyl)boron. *J. Am. Chem. Soc.* **2011**, *133*, 5873−5881.

(6) Heller, E. J. The Semiclassical Way to Molecular Spectroscopy. *Acc. Chem. Res.* **1981**, *14*, 368−375.

(7) Heller, E. J.; Sundberg, R. L.; Tannor, D. Simple Aspects of Raman Scattering. *J. Phys. Chem.* **1982**, *86*, 1822−1833.

(8) Lee, S. Y.; Heller, E. J. Time-Dependent Theory of Raman Scattering. *J. Chem. Phys.* **1979**, *71*, 4777−4788.

(9) Zink, J. I.; Shin, K. S. *Molecular Distortions in Excited Electronic States Determined from Electronic and Resonance Raman Spectroscopy*; Wiley: New York, 1991; Vol. *16*, pp 119−214.

(10) Reber, C.; Zink, J. I. Unusual Features in Absorption Spectra Arising from Coupled Potential Surfaces. *Comments Inorg. Chem.* **1992**, *13*, 177−220.

(11) Wexler, D.; Zink, J. I.; Reber, C. Spectroscopic Manifestations of Potential Surface Coupling Along Normal Coordinates in Transition Metal Complexes. *Electron. Vibronic Spectra Transition Met. Complexes I* **1994**, *171*, 173−203.

(12) Myers, A. B. Resonance Raman Intensity Analysis of Excited-State Dynamics. *Acc. Chem. Res.* **1997**, *30*, 519−527.

(13) Myers, A. B. Resonance Raman Intensities and Charge-Transfer Reorganization Energies. *Chem. Rev.* **1996**, *96*, 911−926.

(14) Myers, A. B. Excited Electronic State Properties from Ground-State Resonance Raman Intensities. *Laser Techniques in Chemistry*; Wiley: New York, 1995; Vol. *23*, p 325.

(15) Kelley, A. M. Resonance Raman Intensity Analysis of Vibrational and Solvent Reorganization in Photoinduced Charge Transfer. *J. Phys. Chem. A* **1999**, *103*, 6891−6903.

(16) Jurss, J. W.; Concepcion, J. J.; Butler, J. M.; Omberg, K. M.; Baraldo, L. M.; Thompson, D. G.; Lebeau, E. L.; Hornstein, B.; Schoonover, J. R.; Jude, H.; et al. Electronic Structure of the Water Oxidation Catalyst cis,cis-$[(bpy)_2(H_2O)Ru^{III}ORu^{III}(OH_2)(bpy)_2]^{4+}$, The Blue Dimer. *Inorg. Chem.* **2012**, *51*, 1345−1358.

(17) Kondov, I.; Vallet, V.; Wang, H. B.; Thoss, M. Ground- and Excited-State Properties of the Mixed-Valence Complex $[(NH_3)_5Ru^{III}NCRu^{II}(CN)_5]^-$. *J. Phys. Chem. A* **2008**, *112*, 5467−5477.

(18) Creutz, C.; Taube, H. Direct Approach to Measuring the Franck-Condon Barrier to Electron Transfer Between Metal Ions. *J. Am. Chem. Soc.* **1969**, *91*, 3988−3989.

(19) Nelsen, S. F.; Weaver, M. N.; Zink, J. I.; Telo, J. P. Optical Spectra of Delocalized Dinitroaromatic Radical Anions Revisited. *J. Am. Chem. Soc.* **2005**, *127*, 10611−10622.

(20) Wootton, J. L.; Zink, J. I. Excited State Distortions in Ligand to Ligand Charge Transfer Excited States of Metal Diimine Dithiolate Mixed Lignad Complexes. *J. Phys. Chem.* **1995**, *99*, 7251−7257.

(21) Talaga, D. S.; Zink, J. I. Choosing a Model and Appropriate Transition Dipole Moments for Time-Dependent Calculations of Intervalence Electronic Transitions. *J. Phys. Chem.* **1996**, *100*, 8712−8721.

(22) Nelsen, S. F.; Konradsson, A. E.; Weaver, M. N.; Telo, J. P. Intervalence Near-IR Spectra of Delocalized Dinitroaromatic Radical Anions. *J. Am. Chem. Soc.* **2003**, *125*, 12493−12501.

(23) Lockard, J. V.; Zink, J. I.; Trieber, D. A.; Konradsson, A. E.; Weaver, M. N.; Nelsen, S. F. Excited-State Mixed Valence in a Diphenyl Hydrazine Cation: Spectroscopic Consequences of Coupling and Transition Dipole Moment Orientation. *J. Phys. Chem. A* **2005**, *109*, 1205−1215.

(24) Nelsen, S. F.; Weaver, M. N.; Luo, Y.; Lockard, J. V.; Zink, J. I. Use of the Neighboring Orbital Model for Analysis of Electronic Coupling in Class III Intervalence Compounds. *Chem. Phys.* **2006**, *324*, 195−201.

(25) Chisholm, M. H.; Lear, B. J. $M_2\delta$ to Ligand π-Conjgation: Testbeds for Current Thoeries of Mixed Valence in Ground and Photoexcited States of Molecular Systems. *Chem. Soc. Rev.* **2011**, *40*, 5254−5265.

(26) Chisholm, M. H. Mixed Valency and Metal-Metal Quadruple Bonds. *Coord. Chem. Rev.* **2013**, *257*, 1576−1583.

(27) Lockard, J. V.; Zink, J. I.; Konradsson, A. E.; Weaver, M. N.; Nelsen, S. F. Spectroscopic Consequences of a Mixed Valence Excited State: Quantitative Treatment of a Dihydrazine Diradical Dication. *J. Am. Chem. Soc.* **2003**, *125*, 13471−13480.

(28) Lockard, J. V.; Zink, J. I.; Luo, Y.; Weaver, M. N.; Konradsson, A. E.; Fowble, J. W.; Nelson, S. F. Excited-State Mixed-Valence Distortions in a Diisopropyl Diphenyl Hydrazine Cation. *J. Am. Chem. Soc.* **2006**, *128*, 16524−16531.

(29) Lockard, J. V.; Valverde, G.; Neuhauser, D.; Zink, J. I.; Luo, Y.; Weaver, M. N.; Nelsen, S. F. Interpretation of Unusual Absorption Bandwidths and Resonance Raman Intensities in Excited State Mixed Valence. *J. Phys. Chem. A* **2006**, *110*, 57−66.

(30) Frisch, M. J.; Trucks, G. W.; Schlegel, H. B.; Scuseria, G. E.; Robb, M. A.; Cheeseman, J. R.; Scalmani, G.; Barone, V.; Mennucci, B.; Petersson, G. A.; et al. *Revision D.01*; Gaussian, Inc.: Wallingford, CT, 2009.

(31) Chisholm, M. H.; Gustafson, T. L.; Turro, C. Photophysical Properties of MM Quadruply Bonded Complexes Supported by

Carboxylate Ligands, MM = Mo_2, MoW or W_2. *Acc. Chem. Res.* **2013**, *46*, 529−538.
(32) McRae, E. G.; Kasha, M. The Molecular Exciton Model. *Phys. Processes Radiat. Biol.* **1964**, 23−42.
(33) Kasha, M.; Rawls, H. R.; Ashraf El-Bayoumi, M. Molecular Spectroscopy. *Proceedings of Eighth European Congress on Molecular Spectroscopy*; Butterworth and Company Ltd.: Boston, 1965; pp 371−392.
(34) Hanna, S. D.; Zink, J. I. Analysis of the Vibronic Structure in the Emission and Absorption Spectra of (μ-1,1-Dicyanoethylene-2,2-dithiolato-S,S')bis(triphenylphosphine)digold(I) and Assignment of the Emissive State. *Inorg. Chem.* **1996**, *35*, 297−302.
(35) Tang, J.; Albrecht, A. C. Developments in the Theories of Vibrational Raman Intensities. *Raman Spectroscopy*; Szynanski, H., Ed.; Plenum Press: New York, 1970; Vol. *2*, pp 33−68.
(36) Warshel, A.; Dauber, P. Calculations of Resonance Raman Spectra of Conjugated Molecules. *J. Chem. Phys.* **1977**, *66*, 5477−5488.
(37) Arivazhagan, M.; Kumar, J. S. Vibrational Assignment, HOMO-LUMO, First-Hyperpolarizability and Mulliken's Charge Analysis of 2,7-Dinitrofluorene. *Indian J. Pure Appl. Phys.* **2012**, *50*, 363−373.
(38) Shriver, D. F.; Dunn, J. B. R. The Backscattering Geometry for Raman Spectroscopy of Colored Materials. *Appl. Spectrosc.* **1974**, *28*, 319−323.
(39) Bailey, S. E.; Cohan, J. S.; Zink, J. I. Interference Effects of Multiple Excited States in the Resonance Raman Spectroscopy of CpCoCOD. *J. Phys. Chem. B* **2000**, *104*, 10743−10749.
(40) Reber, C.; Zink, J. I. Interference Dips in Molecular Absorption Spectra Calculated for Coupled Electronic State Potential Surfaces. *J. Chem. Phys.* **1992**, *96*, 2681−2690.
(41) Shin, K. S. K.; Zink, J. I. Interference Effects on Resonance Raman Excitation Profiles Caused by Two Electronic Excited States. *J. Am. Chem. Soc.* **1990**, *112*, 7148−7157.
(42) Valverde-Aguilar, G.; Wang, X. H.; Plummer, E.; Lockard, J. V.; Zink, J. I.; Luo, Y.; Weaver, M. N.; Nelsen, S. F. Tuning Aryl, Hydrazine Radical Cation Electronic Interactions Using Substituent Effects. *J. Phys. Chem. A* **2008**, *112*, 7332−7341.
(43) Andrade, G. F. S.; Siqueira, L. J. A.; Ribeiro, M. C. C.; Sala, O.; Temperini, M. L. Resonance Raman Effect of Ferrocene and Formylferrocene Thiosemicarbazone. A. *J. Raman Spectrosc.* **2006**, *37*, 498−507.
(44) Ceccarani, M. L.; Sassi, P.; Cataliotti, R. S. Electronic Transitions in Metallocenes by Resonance Raman Scattering. Part 1. Analysis of the Ferrocene Spectrum in the Visible Region. *J. Chem. Soc., Faraday Trans.* **1994**, *90*, 1397−1403.